Journal of
Ship&Ocean Technology
©June 2000

SOTECH Vol. 4, No. 2, pp. 24 ~ 37, 2000

A Study on Upstream Waves for an Advancing Arbitrary Hull Shape in Restricted Water Channel

Sung-Yong Kim[1] and Young-Gill Lee[2]

[1] Department of Naval Architecture, Graduate School, Inha University, Younghyun-Dong, Nam-Ku, Inchon, 402-751, Korea
[2] Department of Naval Architecture and Ocean Engineering, Inha University, Younghyun-Dong, Nam-Ku, Inchon, 402-751, Korea; E-mail: younglee@inha.ac.kr

Abstract

The purpose of this paper is to study the upstream waves in front of an advancing arbitrary hull shape in a restricted water channel. Conventionally, in a restricted water channel, shallow water effects are amplified because of the finite water depth and width. When the effects of shallow water and the restricted channel width are severe, upstream waves propagate forward from the fore-body of the advancing hull. In this study, numerical simulations are carried out for the relevant analysis of the flow phenomena by the draft variation of advancing hull in a restricted water channel. Numerical simulations are done with a finite-difference method based on the MAC scheme in a rectangular grid system.

Keywords: upstream waves, restricted water channel, hull shape, numerical simulations

Nomenclature

F_h	Froude number based on water depth, $F_h = U/\sqrt{gh}$
S_B	blockage coefficient (ratio between transverse channel area and midship section area of ship)
C_B	block coefficient of ship
A	amplitude of first upstream wave
h	water depth of channel
C	average wave celerity
d	draft
U	moving velocity of ship
T	period of upstream wave generation
u	velocity component of longitudinal direction
v	velocity component of transverse direction

w	velocity component of vertical direction
ρ	water density
g	gravitational acceleration
p	pressure
ζ	elevation of free surface
C_P	pressure resistance coefficient

1 Introduction

When a ship is running in a restricted water channel near the critical speed, upstream waves are periodically propagated in front of the ship's bow by the influence of finite water depth and width. That is, these waves are caused by shallow water and blockage effect in the channel. These phenomena cause the high wave making resistance, sinkage and longitudinal trimming of the ship. On occasion, the ship can be stranded. Therefore, the critical speed has to be avoided at the initial design step for a high-speed vessel which will be operating in restricted water conditions. Experiments are employed for the investigation of upstream wave phenomena by Thews and Landweber(1935). In addition, Izubuchi and Nagasawa(1937), Graff et al(1962) had performed the experimental research on these phenomena. However, they could not explain source of the phenomena. In these circumstances, by systematic experimental researches with Huang et al(1982) and Ertekin et al(1984), these problems also have become principal research topics of nonlinear free-surface waves. The research of Wu and Wu(1982) was the first theoretical approach that was performed for the calculation of the generation and propagation of upstream waves with a moving disturbance spanning uniformly across the channel by using the generalized Boussinesq equation. After that, many other researchers have performed the theoretical study for the upstream waves in restricted water conditions. For example, Bai and Kim(1989) computed the flow problem for a ship moving in a numerical towing tank by using a finite-element method, and Ertekin and Qian(1989) solved the problem of a vertical strut moving in a restricted water channel with a finite-difference method. From the computational results, the surface elevation and wave resistance were compared with several appropriate experimental data. Also, the wave resistance and the amplitude of upstream waves about a slender ship advancing near the critical speed in restricted water condition were studied by Choi and Mei(1989). They used an asymptotic expansion technique showing that the response of open channel flow can be described by the homogeneous Kadomtsev-Petviashvili equation.

In the engineering field of naval architecture, those problems are concerned with the increases of the wave resistance and trim of a ship going through restricted water channel. Also, the analysis of flow characteristics around the hull form plays an important role for the design of canal-going ships. One of the most exciting aspects in this identified phenomenon is that a three-dimensional disturbance, such as a model ship, generates two-dimensional propagating waves in a towing tank with finite width. In addition, the propagation speed of upstream waves is greater than the constant towing speed of ship model so that a steady state cannot be attained. Most of existing numerical researches are interested in free-surface simulation based on potential flow theory. However, in this paper the cause of upstream wave generation and the generating procedures are fundamentally investigated by numerical simulation method.

2 Numerical Simulation Method

2.1 Governing equation

In this study, the flow is assumed to be incompressible and inviscid. Hence conservative three-dimensional Euler equations and continuity equation are adopted for the governing equations as shown in (1) and (2).

$$\begin{aligned} \frac{\partial u}{\partial t} + \frac{\partial (u^2)}{\partial x} + \frac{\partial (uv)}{\partial y} + \frac{\partial (uw)}{\partial z} &= -\frac{1}{\rho}\frac{\partial p}{\partial x} \\ \frac{\partial v}{\partial t} + \frac{\partial (uv)}{\partial x} + \frac{\partial (v^2)}{\partial y} + \frac{\partial (vw)}{\partial z} &= -\frac{1}{\rho}\frac{\partial p}{\partial y} \\ \frac{\partial w}{\partial t} + \frac{\partial (uw)}{\partial x} + \frac{\partial (vw)}{\partial y} + \frac{\partial (w^2)}{\partial z} &= -\frac{1}{\rho}\frac{\partial p}{\partial z} + g \end{aligned} \tag{1}$$

$$\frac{\partial u}{\partial x} + \frac{\partial v}{\partial y} + \frac{\partial w}{\partial z} = 0 \tag{2}$$

Here, u,v and w are the velocity component in each direction, ρ is the water density, g is the gravitational acceleration, and p is the pressure.

A staggered grid system with variable mesh is employed to improve the convergency and accuracy of the simulation results. The computational domain is composed of the flow fields around half of the ship and symmetric boundary conditions are required on the center plane. Cartesian coordinate system is employed and its origin is located on the intersection of forward perpendicular and the free-surface of the calm water. In this numerical method, the governing equations are represented in finite-difference forms by forward differencing in time and second-order centered differencing in space except for its convective terms, and these are solved as initial value and boundary value problems by using the time marching procedure and iterative methods. The computational procedure is similar to the previous study by Nishimura and Miyata(1985) except for the introduction of the bottom and side boundary conditions.

2.2 Boundary conditions

2.2.1 Body boundary condition

In this numerical method, all cells are either a fluid cell, a body boundary cell or a empty cell, and appropriate calculation methods are prepared for the each type of cell. Hull surface is approximated by continuous line segments in XY plane for the water lines and stair shapes in YZ plane for the station lines. Free-slip condition is adopted to satisfy the body boundary condition, and a velocity-pressure simultaneous iterative method is used for the calculation of pressure in each body boundary cell.

2.2.2 Free-surface boundary condition

The kinematic and dynamic conditions are imposed on the free-surface as follows:

$$\frac{D(\zeta - z)}{Dt} = \frac{\partial \zeta}{\partial t} + u\frac{\partial \zeta}{\partial x} + v\frac{\partial \zeta}{\partial y} - w = 0 \tag{3}$$

$$p = p_0 \tag{4}$$

where, ζ is the elevation of free-surface, and p_0 is the atmospheric pressure.

On the free-surface boundary, surface tension and viscous stress are neglected and the dynamic boundary condition is fulfilled by the *irregular star* technique for the calculation of pressure in the cells near the free-surface. At each time step, the configuration of the free-surface is determined by the location of marker particles which are moved in a Lagrangian movement manner. That is, the kinematic boundary condition is fulfilled with this marker movement on the free-surface.

2.2.3 Other boundary conditions

Other boundary conditions are utilized as follows. In inflow boundary, Dirichlet and Neumann conditions are adopted for the boundary values of velocity and pressure, respectively. On the centerplane of ship, the symmetric boundary condition is adopted. Also, in the case of the outflow boundary condition, Neumann condition is used for the boundary values of velocity and pressure field. For the numerical flow simulation of restricted water channel, side and bottom boundary conditions are applied by slip boundary condition for velocity field and Neumann condition is adopted for the pressure field.

3 Numerical Computation Results and Discussion

Numerical simulations are carried out for an arbitrary hull shape (Case 1) and a model ship of a Series 60, C_B=0.80 hull (Case 2). In the case of the arbitrary hull shape, the transverse hull section ratio is varying in a two-dimensional parabolic manner in the longitudinal direction and the breadth of the hull is the same at each water line. Numerical computations are performed with the running condition of model ship in deep water, shallow water and restricted water channel. The Froude Number (F_h) is defined by the ship's speed and the water depth of the channel. The blockage coefficient (S_B) is the ratio of the ship's cross-sectional area at midship to the cross sectional area of the water channel. Present simulations are performed from the case of $F_h = 1.0$ and $S_B = 0.09 \sim 0.13$. In this critical speed and restricted condition, the ship has the maximum propagating angle of divergent waves at fore-body. Table 1 shows the computational conditions of two cases, and Figure 1 shows the schematic drawing of computational conditions. A sample calculation with a strut model (Case 1) is performed to validate the numerical scheme of the present finite-difference method. Wave patterns around the arbitrary hull shape (strut) and the evolution of upstream waves with the advance of time are represented in Figure 2. In this figure, upstream waves are periodically generated at the fore-body of the strut and the wave height is reduced greatly at the aft-body in the opposite manner. The wave height at the rear side is reduced because of mass transportation from the flow field around the aft-body to the flow field around the fore-body. Therefore, this computational result is considered to be reasonable.

The time-sequential variation of the two-dimensional wave pattern on the side-wall of the channel is shown in Figure 3. This figure shows a periodical wave generation from the fore-body and the wave height at the rear side is reduced in the opposite manner. These flow phenomena cause the large sinkage and longitudinal trim of the ship. For the same period, the curve of pressure resistance coefficient is shown in Figure 4. The pressure resistance coefficient is $C_P = R_P/(\frac{1}{2}\rho S V^2)$, where R_P is the pressure resistance of ship, ρ is the density of water, S

Table 1: Computational conditions

	Strut (Case 1)	Series60, $C_B = 0.80$ (Case 2)
Channel Width	2	1.22
Channel Depth	0.25	0.15
Ship Length	2	1.524
Ship Breadth	0.4	0.234
Draft(d)	0.131	0.10, 0.075
F_h	1.0	1.0
S_B	0.105	0.126, 0.095

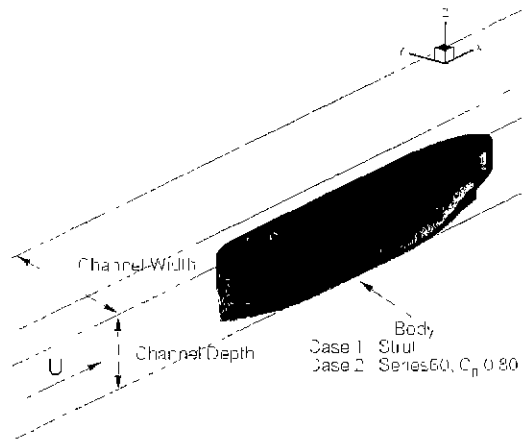

Figure 1: Schematic drawing of computational conditions

and V are the wetted surface area and velocity of ship, respectively. In this figure, the values of pressure resistance coefficient periodically fluctuate with the upstream wave generation.

Time history of pressure distributions along the center plane and at the side-wall of the restricted water channel are shown in Figure 5. This figure shows that the pressure value increases steadily around the fore-body during the generation of the first upstream wave, and the pressure value on both side-walls increases as the waves spread to both side-walls. In these results, the flow rate between the hull and the side-walls of the restricted water channel at the longitudinal position of the fore-body gradually decreases. These flow phenomena cause the increase of mass and wave height in the flow field around the fore-body. After this stage, the wave height at the side-walls that was increased in the earlier stage decreases because of the gravitational effect and the higher pressure region as a result of the higher speed of the ship as shown in Figure 5. These flow phenomena are periodically repeated when the upstream waves are generated.

In Table 2, the present simulation results are compared with several existing calculation results about periodical wave amplitude, propagation speed and period. Firstly, the present result shows about 14% lower value in case of the wave amplitude. It is considered that the discrepancy is

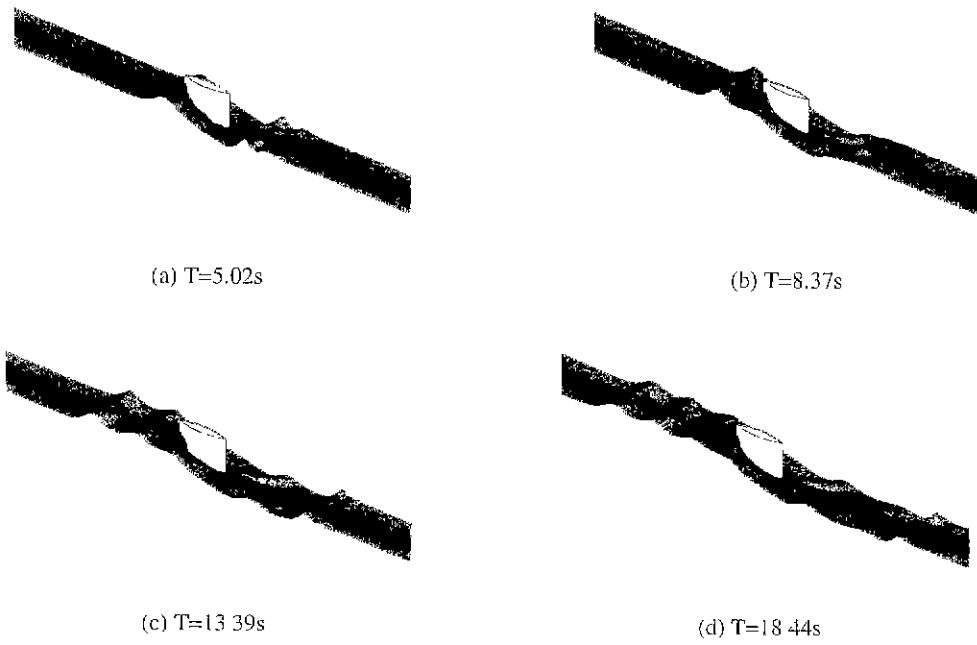

(a) T=5.02s (b) T=8.37s

(c) T=13 39s (d) T=18 44s

Figure 2: Evolution of wave field generated by strut (Case 1)

Table 2: Comparisons of wave amplitude, propagation speed and period (Case 1)

	A/h	$C/\sqrt{gh}$	UT_s/h
Bai and Kim	0.553	1.24	30.0
Ertekin and Qian	0.624	1.28	29.6
Choi and Mei	0.562	1.28	28.8
Present result	0.480	1.22	30.1

induced from the difference of the hull shape and breadth on the free-surface. In the case of wave propagation speed, the present result is about 5% lower from others and the wave generation period has about 2% deviation with other results. It is considered that these differences are fundamentally caused by the difference of numerical calculation methods and the shape of the hull section. In Figure 6, it shows the perspective views of wave formation around the Series 60 hull shape in deep water and shallow water conditions. In this figure, the characteristics of the wave pattern in shallow water condition are shown. That is, it is shown that the divergent angle and height of bow waves increase in the shallow water condition compared to those of the deep water condition. Figure 7 shows the pattern of upstream wave generated by Series 60 hull shape at a set of selected sequential time intervals. Generally speaking, the pattern of wave generation is similar to former case (Case 1), but it has some differences about the time and period for the upstream wave generation.

The two-dimensional wave patterns on the side-walls of the restricted water channel according to each computational condition and time steps are shown in Figures 8 and 9. In these results,

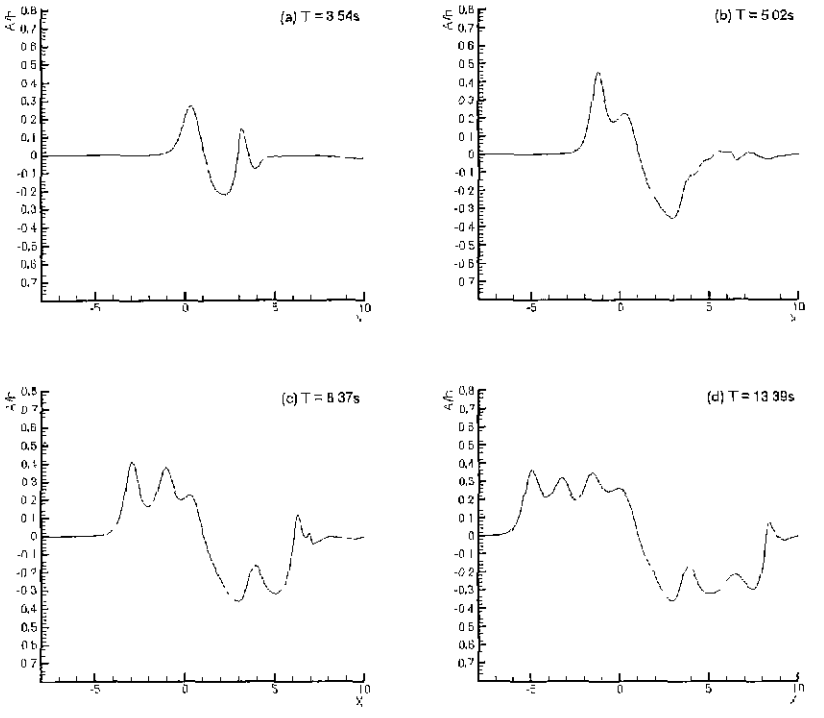

Figure 3: Wave height profiles on the side-wall of channel (Case 1. $F_h = 1.0$, $S_B = 0.105$)

the height and period of the upstream waves are shown at two different drafts. In this case, the increment of ship's draft causes the increment of blockage coefficient (S_B), then the time and period of upstream wave generation are accelerated. The present results have the same patterns as those of the existing experiment(Huang et al 1982). The pressure resistance coefficients integrated on the hull surface at each computational condition are shown in Figure 10. These curves show the variation of pressure resistance coefficients for various combinations of the bottom and side conditions in computational domain. The pressure resistance values in the shallow water and restricted water channel conditions are larger than that of the deep water condition. Increasing the draft shows the same trend in the pressure resistance. The pressure resistance coefficient varies with the same period as that of the wave generation period at the bow of ship. Wave generation period changes with the draft of the ship.

In Table 3, the computed result for the Series 60 hull shape are compared with the experimental result(Ertekin et al 1984). The wave amplitude in this calculation is 9% lower than the experimental results and the period is larger by 1%. The difference might be caused by the uncertainty of experimental measurements and also by the inaccuracy in the hull surface definition in the calculation procedure. The locations of numerical wave height gauges are shown in Figure 11, which is to be compared with the experimental results of Ertekin et al(1984). The wave heights are recorded at the designated time steps and positions by using the numerical wave height gauges.

The wave heights at each position of gauges are compared with the results of existing experiment(Ertekin et al 1984) as shown in Figure 12. The computed period of upstream waves at the

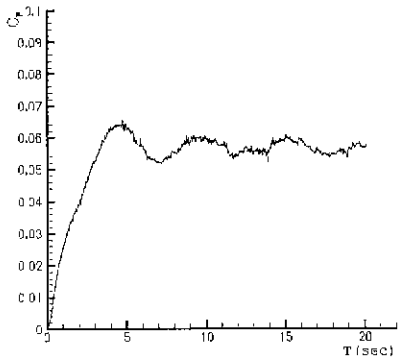

Figure 4: Time history of pressure resistance coefficient (Case 1)

Table 3: Comparisons of wave amplitude and period (Case 2, d=0.075)

	A/h	UT/h
Ertekin et al	0.54	38.0
Present result	0.49	38.4

four position of gauges shows good agreement with experiment, but the wave height shows some difference with the experimental data. The difference could be caused by the uncertainty in the experimental measurements and also by the adopted finite difference schemes in the present numerical procedure. The numerical prediction agrees well qualitatively with experimental results. The flow simulation in restricted water channel, however, requires further improvement not only for the upstream waves at fore-body but also for the nonlinear flow around after aft-body. The present numerical simulation method is evidently a useful alternative to experiments especially for the case when the flow observation in the experimental tanks is very difficult.

4 Conclusions

1. In this paper, numerical simulations when a ship is running in restricted water channel at the critical speed are carried out for the investigation of flow phenomena. The free-surface variation and the generation procedure of upstream waves are explained for the understanding of flow characteristics in the restricted water channel.

2. The numerical simulation results are qualitatively in a good agreement with other existing calculated and experimented data.

3. It was found that the present numerical simulation method is a useful tool for the investigation of flow characteristics in the restricted water channel that is difficult to study using experiments.

4. Further improvement in treating the body segment geometry in the vertical direction and also the inclusion of the viscous effect in fluid region will make the present numerical simulation method be a useful tool for the study of nonlinear free-surface problems.

Acknowledgements

This work was supported in part by the Korea Science and Engineering Foundation (KOSEF) through the Regional Research Center for Transportation System of Yellow Sea at Inha University.

References

BAI, K. J. AND KIM, Y. H. 1989 Numerical Computations for a nonlinear free surface flow problem. Proc, Fifth Int'l Conf on Numerical Ship Hydrodynamics, Hiroshima, Japan, Part 2, pp. 305-320

CHOI, H. S. AND MEI, C. C. 1989 Wave resistance and squat of a slender ship moving near the critical speed in restricted water. Proc, Fifth Int'l Conf on Numerical Ship Hydrodynamics, Hiroshima, Japan, Part 2, pp. 337-350

ERTEKIN, R. C. AND QIAN, Z.-M. 1989 Numerical grid generation and upstream waves for ships moving in restricted waters. Proc, Fifth Int'l Conf on Numerical Ship Hydrodynamics, Hiroshima, Japan, Part 2, pp. 321-336

ERTEKIN, R. C., WEBSTER, W. C. AND WEHAUSEN, J. V. 1984 Ship-generated solitons. Proc. 15th Symp on Naval Hydrodynamics. Hamburg, pp. 347-361

GRAFF, W. 1962 Untersuchungen uber die Ausbildung des Wellenwiderstandes im Bereich der Stauwellengeschwindigkeit in Flachem. Seitlich Beschranktem Fahrwasser. Shiffstechnik, **9**, pp. 110-122

HUANG, D.-B., SIBUL, O. J. AND WEHAUSEN, J. V. 1982 Ships in very shallow water, FestkolloQuium Zur Emeritierung von Karl Wieghardt. Institut fuer Schiffbau, Hamburg Univ. Bericht, **427**, pp. 29-49

IZUBUCHI, T. AND NAGASAWA. 1937 Experimental investigation on the influence of water depth upon the resistance of ships. J. of Society of Naval Architects of Japan, **61**, pp. 165-206

LEE, Y.-G., MIYATA, H. AND KAJITANI, H. 1988 Some application of the TUMMAC method to 3D water-wave problem. J. of Society of Naval Architects of Korea, **25**, **4**

NISHIMURA, S. AND MIYATA, H. 1985 Finite difference of nonlinear ship waves by the TUMMAC-IV method and its application to hull-form design. J. of Society of Naval Architects of Japan, **157**

THEWS, J. G. AND LANDWEBER. 1992 The Influence of shallow water on the resistance of a cruiser model. U. S. Experimental Model Basin, Navy Yard, Washington, D. C., **408**

WU, D. M. AND WU, T. Y. 1984 Three-dimensional nonlinear long waves due to moving surface pressure. Proc, 14th Symp on Naval Hydrodynamics, Ann Arbor, pp. 103-129

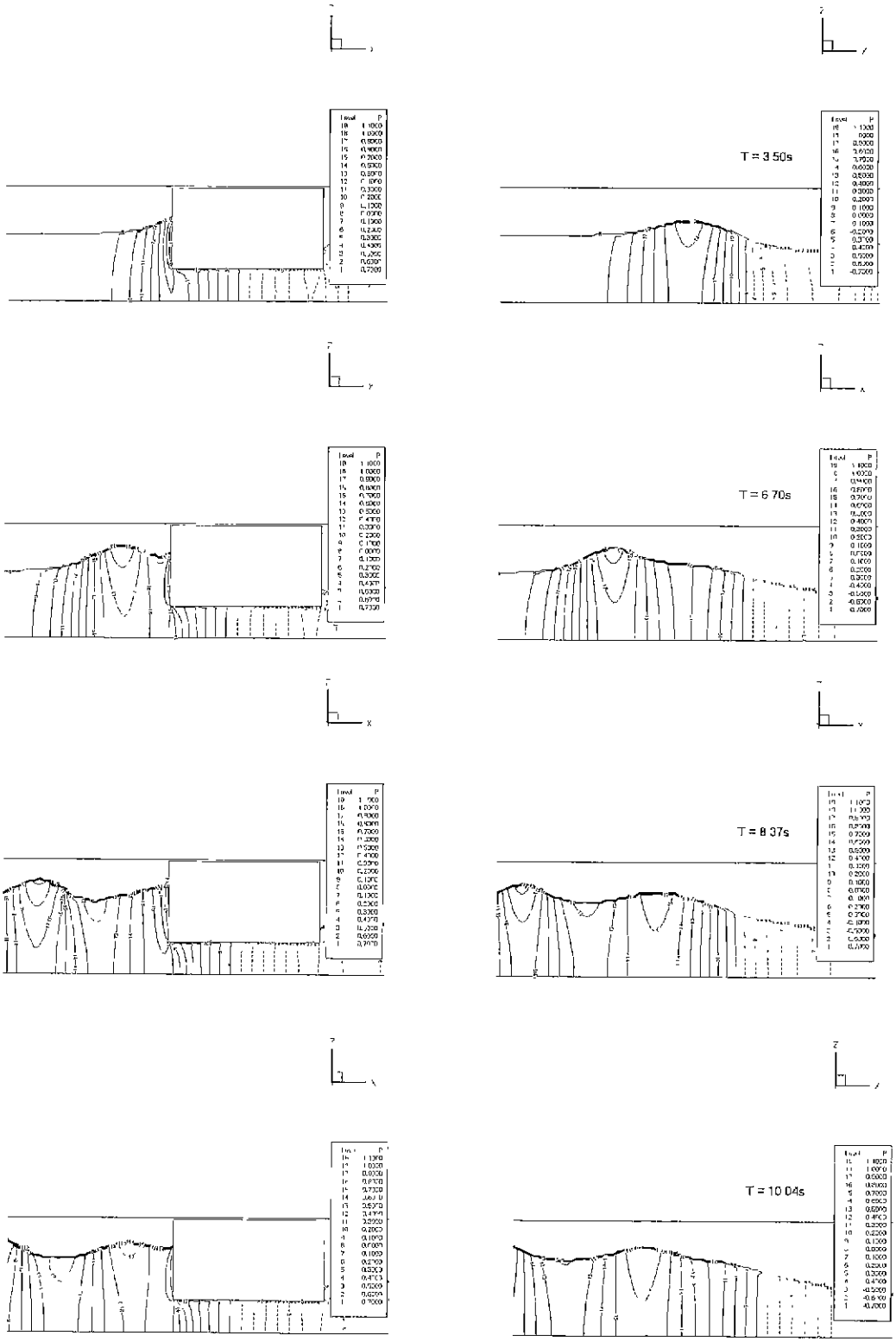

(a) Center plane (b) Side wall

Figure 5: Pressure contours on the center plane and side wall of channel (Case 1)

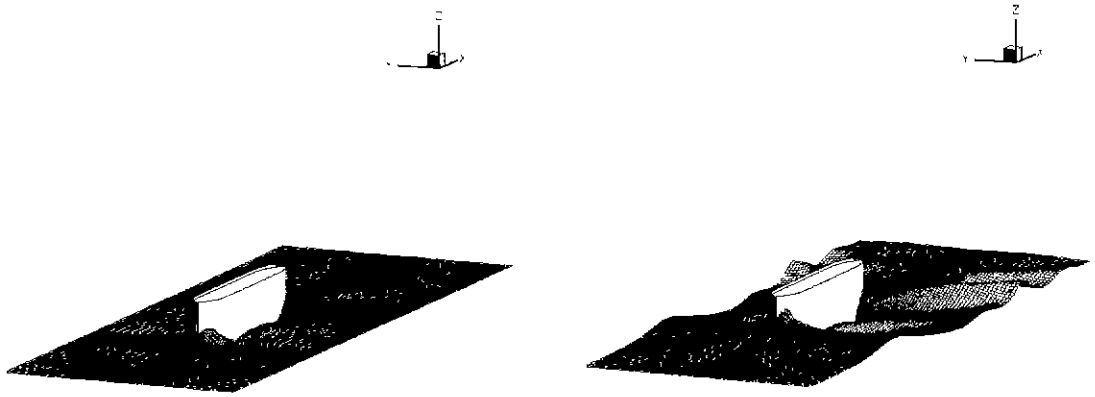

(a) Deep water condition

(b) Shallow water condition

Figure 6: Comparison of the wave pattern between deep water and shallow water for a Series 60 hull with C_B=0.80

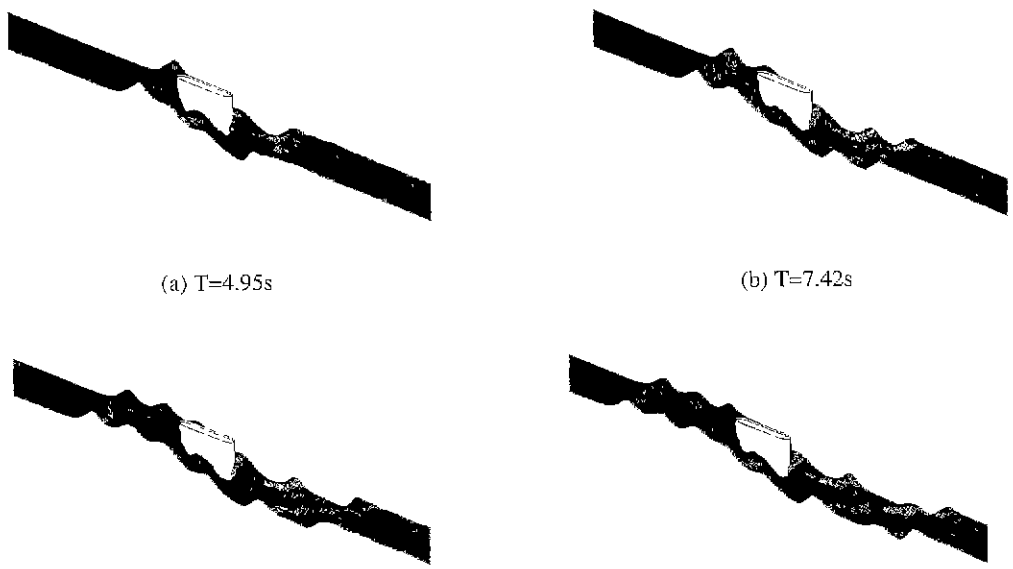

(a) T=4.95s

(b) T=7.42s

(c) T=9.90s

(d) T=12.37s

Figure 7: Evolution of the wave field generated by a Series 60 hull with C_B=0.80, d=0.10 (Case 2)

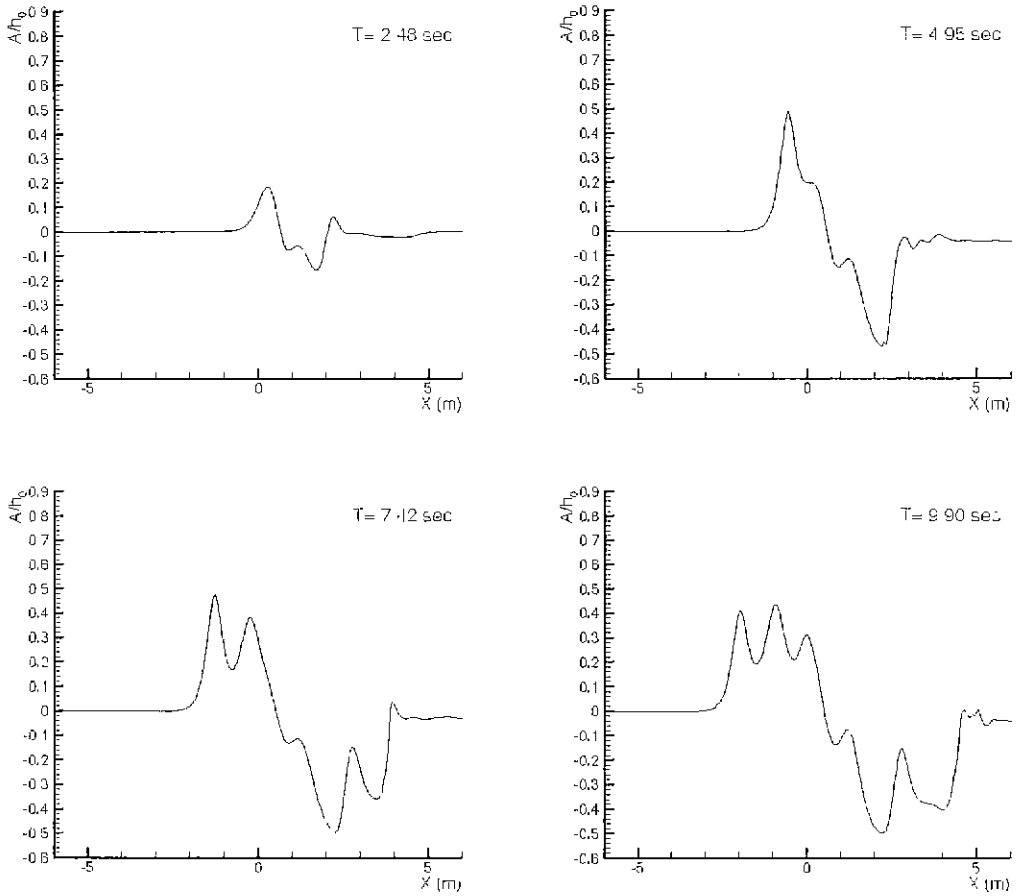

Figure 8: Wave height profiles (Series 60, C_B=0.80, d=0.10)

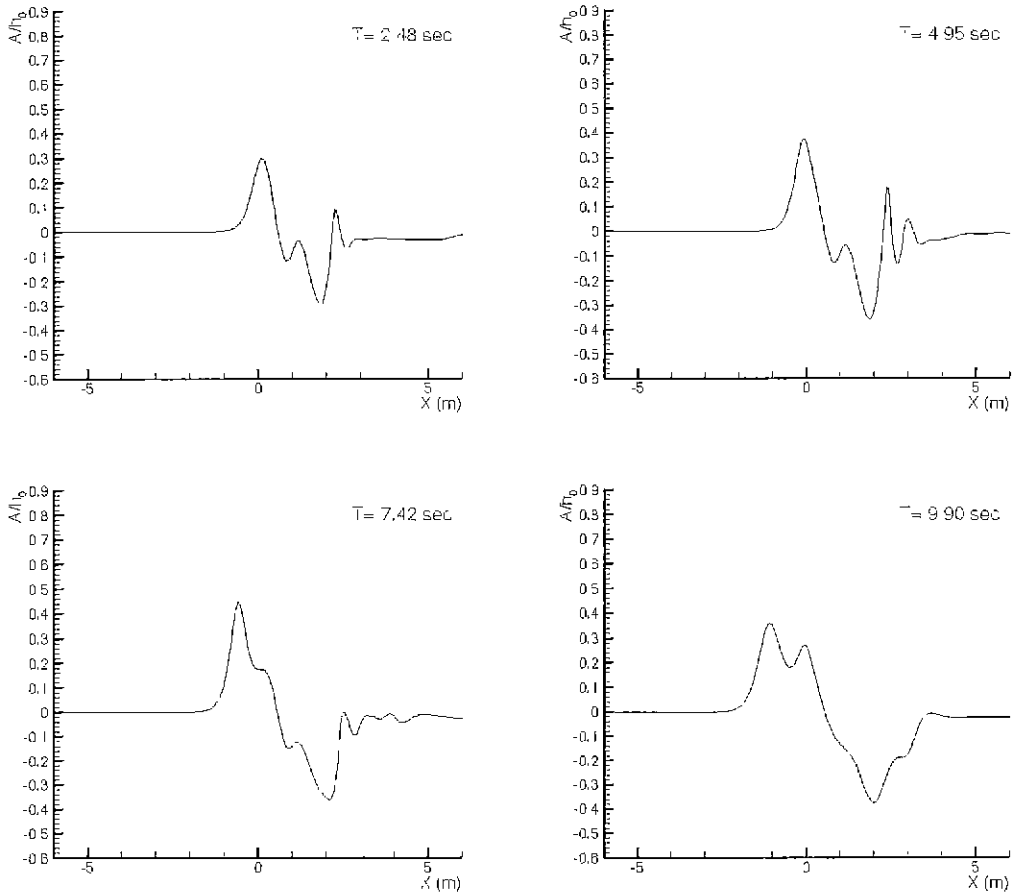

Figure 9: Wave height profiles (Series 60, C_B=0.80, d=0.075)

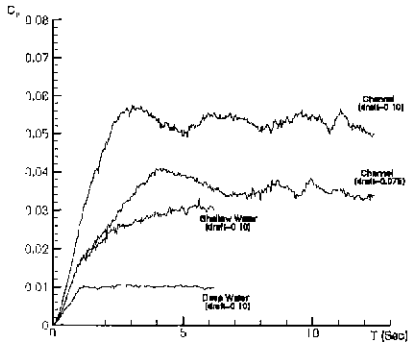

Figure 10: Comparisons of pressure resistance coefficients

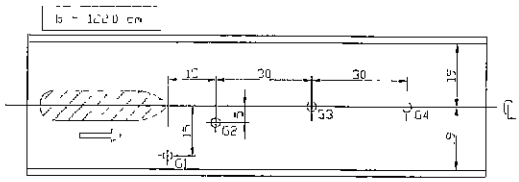

Figure 11: Location of wave height gauges (Series 60, C_B=0.80)

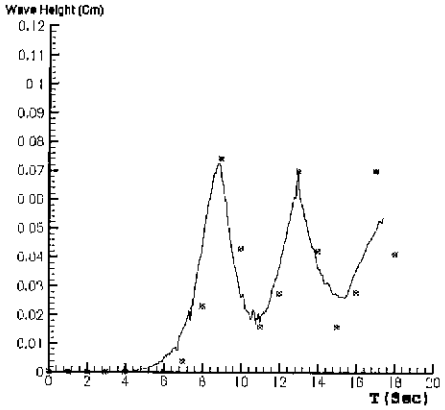

(a) Gauge 1(G1)

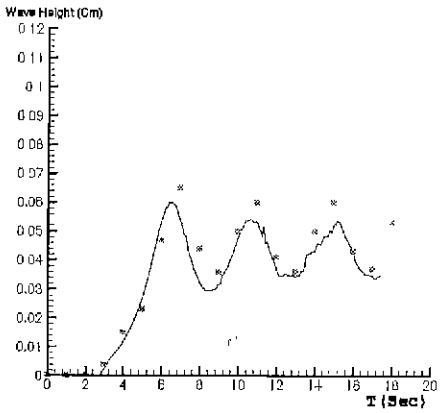

(b) Gauge 2(G2)

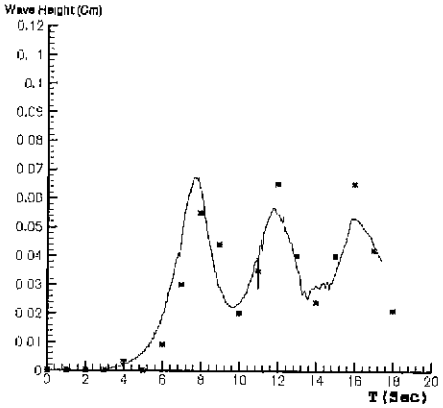

(c) Gauge 3(G3)

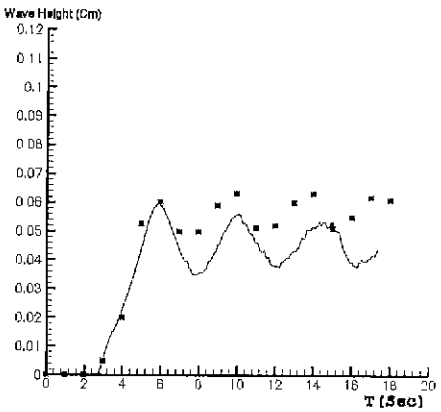

(d) Gauge 4(G4)

Figure 12: Evolution of the wave field generated by Series 60 C_B=0.80, d=0.10 (Case 2)